CFD investigation of backward - facing step nanofluid flow

CFD investigation of backward - facing step nanofluid flow

M M Klazly[1] and G Bognár[1]

[1] University of Miskolc, Department of Machine and Product Design, 3515, Miskolc-Egyetemváros, Hungary

E-mail: v.bognar.gabriella@uni-miskolc.hu

Abstract. Heat transfer enhancement of different nanofluid laminar flow over backward facing step is numerically studied in this paper. The expansion ratio is chosen according to the experimental setup suggested by Armaly H/h = 1.9432. The Reynolds number is taken in a range of $10 \leq Re \leq 400$. The result showed a primary recirculation region developed after the sudden expansion before it starts to change to become fully developed flow downstream of the reattachment point. The length of the reattachment point increases as Reynolds number increases. The effect of the volume fraction has observed along the downstream wall for Al_2O_3 - water nanofluid. Moreover, the impact of the volume fraction on the thermal boundary layer and heat transfer is investigated.

1. Introduction

The flow separation and reattachment of the fluid is one of the common phenomena that happen in many engineering applications. Backward facing step geometry, where the flow separation happens due to a sudden expansion is one of the structures that can be found in heating and cooling devices such as: nuclear reactors, combustion chambers, flow in valves, cooling compressors blade, electronic cooling equipment, wide angle diffusers, and high-performance heat exchangers. The separation of the flow is unwanted in many of the previous examples due to the pressure drop, which causes energy losses by the additional fan or pumping power. However, in some applications for instance in the burner flame stabilization, the flow separation can enhance the heat transfer, where it is used for turbulence promotion.

In 1950, a study on the separation and reattachment flow over a backward facing (BWF) step was conducted, which was considered as the first study and effort on the BWF flow. Then, due to the improvement in the numerical codes and computational tools the number of researches has started to investigate more types of geometrical and boundary conditions such as horizontal, inclined and vertical cases. A review on the fluid flow and heat transfer using a single phase for laminar mixed convective flow over different orientations steps is made by Abu-Mulaweh [1].

The 2D backward facing step forced convection flow behaviour has been studied both experimentally and numerically. Denham and Patrick studied the flow without investigating the heat transfer effects [2]. In the experimental work, Armaly found that the reattachment point position moves downstream far from the sudden expansion as Reynolds number increases [3]. Furthermore, Shih, Chiang, and others investigated the 3D forced convection flow; the result of their studies shows that the reattachment zone is greater near the sidewall compared to the centre plane of the channel [4-12]. Also, the heat transfer

phenomena over the BWF is investigated extensively in the literature. This phenomenon has an influence on the fluid flow characteristics due to the buoyancy force. The horizontal flow has shown an irrelevant effect on the buoyancy effect compared to inclined and vertical flow due to the height limitation. The authors of the experiment and numerical works for the 2D airflow over a horizontal BWF heating with uniform heat flux or constant wall temperature have reported that the higher value of the local Nusselt number was noticed to be near the reattachment point while the lower value close to the step, and the recirculation region and Nusselt number decreases as the buoyancy force increases [13-17].

The 3D backward-facing step has been investigated using various parameters [18-24]. The results showed that the maximum local Nusselt number observed at the area of the reattachment point approximately between the centre-plane and the sidewall. Moreover, the effect of the backward facing step duct orientation was studied [25-29]. The authors reported that the inclination angle between 0° to 180° has a significant effect on the reattachment length, where the increase in the inclination increases the reattachment length and decrease the wall fraction and Nusselt number. However, the opposite behaviour was noticed between 180° to 360° on the reattachment length and Nusselt number. The flow and heat transfer of nanofluid over a backward facing step behaviour was studied for the first time by Abu-Nada [30]. He investigated Reynolds number between 200 and 600 with volume fraction 0 to 0.2 the study includes five different mixtures of nanofluids. In the literature, the number of studies dealing with such a problem is slightly small.

Our goal is to investigate the flow behaviour and heat transfer for a higher concentration of nanoparticles flows. In section 2, the governing equations describe the model are given. In section 3, the geometry generated, the mesh dependency study and the numerical solution method are presented in section 4. The numerical simulations for forced convective flow over a BWF are carried out using different volume fractions. Our aim is to examine the velocity distribution, walls shear and the heat enhancement of the heat transfer at the bottom wall.

2. Model description and governing equations

The computational domain is schematically shown in Figure 1. The expansion ratio has been chosen as H/h=1.9432, and the length of the upstream wall, and downstream were Lu = 5 m, and Ld =10 m, respectively. The flow at the inlet was considered to be hydrodynamically steady with temperature of 274 K and the velocity specified by Reynolds number $10 \leq Re \leq 400$. The downstream stepped wall was heated with constant temperature of 400 K, and all the other walls were fixed to be adiabatic. The single-phase approach for solving the flow of nanofluid problem is adopted in this numerical study. In this approach the following assumptions are used:

- The nanoparticles and the base fluid (water) are to be perfectly mixed and treated as a homogenous mixture. Moreover, the fluid phase and the solid particles are assumed to be in thermal equilibrium and move with the same velocity.
- Steady, Newtonian and incompressible fluid flow is considered.
- The thermophysical properties of the nanofluid are temperature independent and assumed to be dependent on the volume fraction of the nanoparticles.

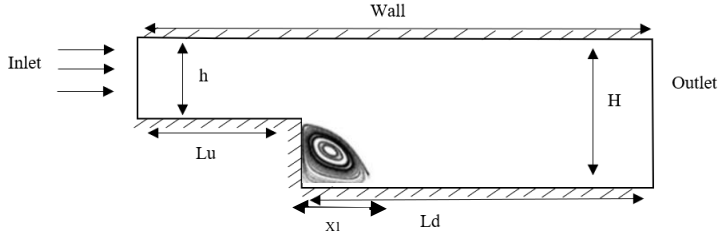

Figure 1. The schematic diagram of the computational domain

2.1. Governing equations

Equations (1) to (3) are continuity, momentum, and energy governing equations that present the mathematical formulation of the single-phase model [39][40].

$$div\left(\rho_{nf}\vec{V}\right) = 0 \quad (1)$$

$$div\left(\rho_{nf}\vec{V}\vec{V}\right) = -\nabla P + \mu_{nf}\nabla^2\vec{V} \quad (2)$$

$$div\left(\rho_{nf}\vec{V}C_{pnf}T\right) = div\left(k_{nf}\nabla T\right) \quad (3)$$

where the following notations are used:

$\vec{V}$, P, and T present the velocity vector, pressure, and temperature, respectively. μ_{nf} is the viscosity of nanofluid, ρ_{nf} is density of the nanofluid, k_{nf}, and C_{pnf} are the thermal conductivity and thermal capacity, respectively.

2.2. Thermal properties of the nanofluid

The thermal properties of the nanofluid are modelled as a function of the volume fraction. The viscosity, density, thermal capacity, and the thermal conductivity are approximated depending on the concentration of the nanoparticles in the base fluid using equation (4)-(7) as defined in [31-36]. Table 1. Shows the thermo-physical properties for Al_2O_3-water at a different values of ϕ [37].

$$\mu_{nf} = \frac{\mu_b}{(1-\phi)^{2.5}} \quad (4)$$

$$\rho_{nf} = (1-\phi)\rho_b + \phi_p\rho_p, \quad (5)$$

$$C_{pnf} = \frac{\phi(\rho C_p)_p + (1-\phi)(\rho C_p)_b}{\rho_{nf}}, \quad (6)$$

$$k_{nf} = k_b \frac{k_p + 2k_b - 2\phi(k_b - k_p)}{k_p + 2k_b + \phi(k_b - k_p)}. \quad (7)$$

Table 1. The thermo-physical properties of water-Al2O3 at different value of ϕ

Parameter	**Pure water (0%)**	**Al_2O_3-water (1%)**	**Al_2O_3-water (2%)**	**Al_2O_3-water (3%)**	**Al_2O_3-water (4%)**
$\rho[kg/m^3]$	997.1	1026.829	1056.558	1086.287	1116.016
$C_p[J/kg.K]$	4179	4047.005	3922.4389	3804.6906	3693.2155
k[w/m.K]	0.613	0.63073914	0.6488238	0.6672642	0.6860711
μ[Pa.s]	0.001	0.001025444	0.001051180	0.001079122	0.001107444

3. Numerical procedure and validation

3.1. Geometry

The geometry is generated by using ICEM CFD, and the two-dimensional flow problem was chosen according to the experimental setup published by Armaly et al [3], where H/h=1.9432 is the expansion ratio. H is the channel height downstream, and h is the height of the inflow channel. In the present study, all the geometrical length is made based on the channel height, L_u =5h is the upstream channel length, while L_d =10 h is the downstream channel length.

3.2. Mesh grid testing and model validation

Non-uniform quadrilateral grid system is employed for meshing the domain generated by Blocking method in ICEM CFD as shown in Figure 4. The grid is centred on the walls and the step will give greater simulation accuracy and more efficient computing time. The maximum face size of the mesh was 0.005 m and the maximum aspect ratio 1:2. Four different meshes represent the criteria of grid independency at Re=100 (see Table 1).

The purpose of this mesh dependency study for X1 is to avoid the result relying on the mesh. After the 3rd mesh, the grid difference is less than 1%, which can be considered as grid-independent. For further validation, the result of the reattachment point compared to Armaly's work, where the result showed excellent agreement, as shown in Figure 3.

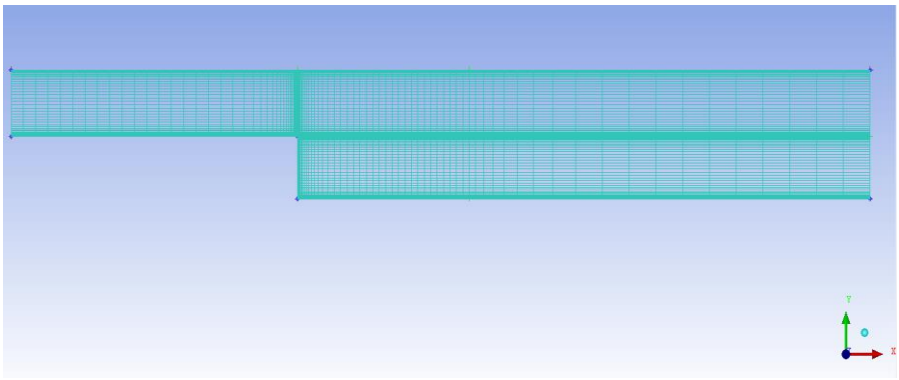

Figure 2. Mesh generation for the model

Table 2. The grid independency

Mesh	Size	X1
1	25*80	2.6891
2	35*90	2.7078
3	40*100	2.7191
4	50*110	2.7192

3.3. Numerical solution method

A finite volume method (FVM) was used for discretizing the equations of mass, momentum, and energy. ANSYS fluent solver used to perform the calculations by solving the system of equations (1) – (3) together with the boundary conditions. The solution method was as follows: a simple algorithm was used to resolve the velocity-pressure coupling. The convection and diffusion terms in the governing equations were discretized using a second-order upwind scheme. The convergence criteria of the solutions monitored by a residual monitor of 10^{-6}.

3.4. Validation

The streamlines of the steady state flow of water are compared with the results of Armaly's flow field for the same expansion ratio. For Reynolds number Re=10 the flow follows the upper convex corner without revealing a flow separation and a corner vortex is formed in the concave corner after the step. Figure 4 shows the experimental and numerical simulation result for Re =10. Moreover, for a higher value of Reynolds number, the corner vortex strongly increases in size. At Re=50 it can be seen that the corner vortex reaches up to the corner of the step and covers the complete face of the step. For Re=100 the same behaviour is observed, i.e., with increasing the Reynolds number the size of the recirculation region steady increases. Figure 3 exhibits the variation reattachment length as a function of the Reynolds number and the excellent agreement of the present simulation with the experimental results of Armaly, and Biswas [3], [38].

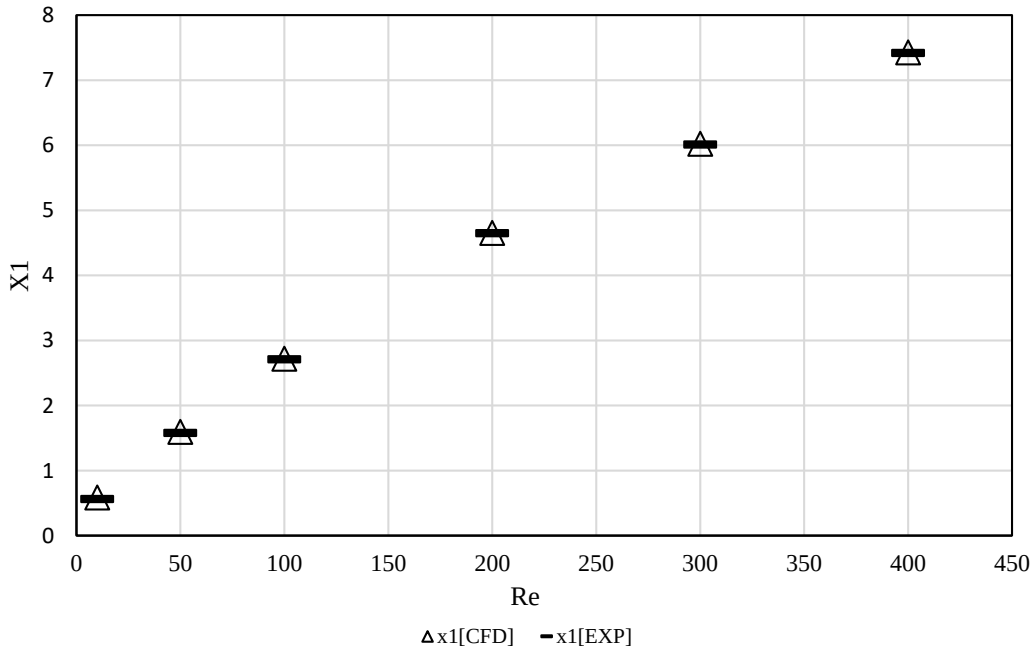

Figure 3. Comparison length X1 of present study with Armaly's experimental results

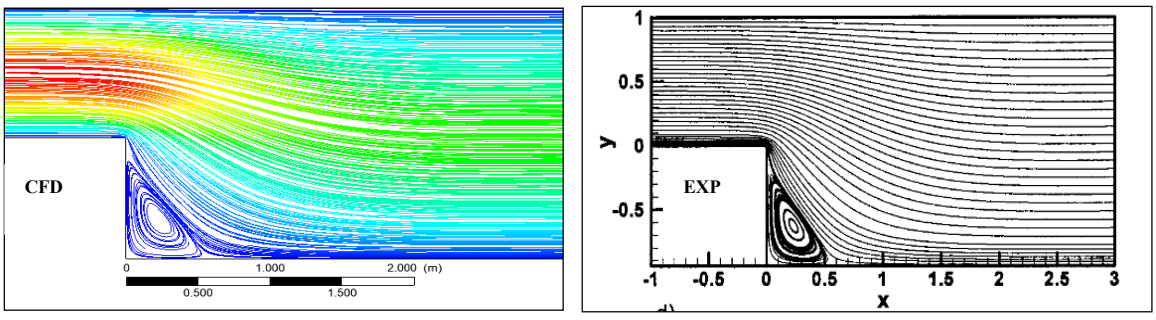

Figure 4. Stream line patterns for the flow separation at Re=10

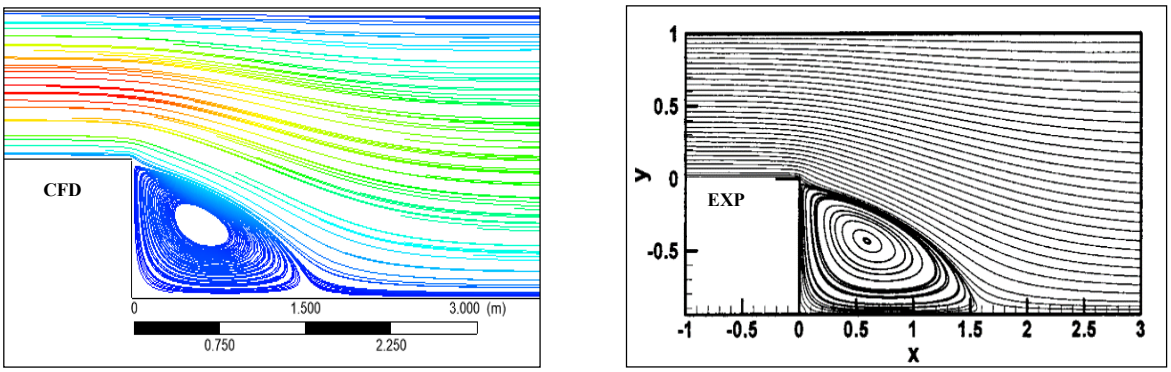

Figure 5. Stream line patterns for the flow separation at Re=50

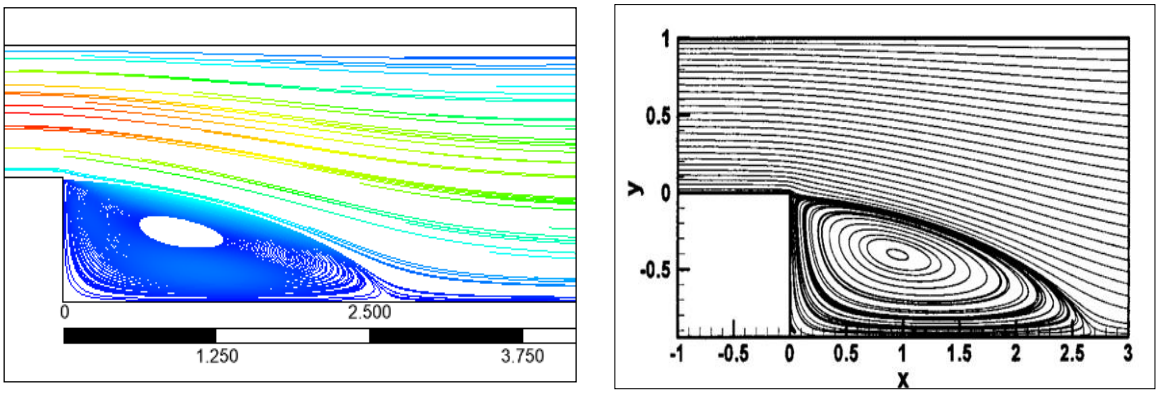

Figure 6. Streamline patterns for the flow separation at Re=100

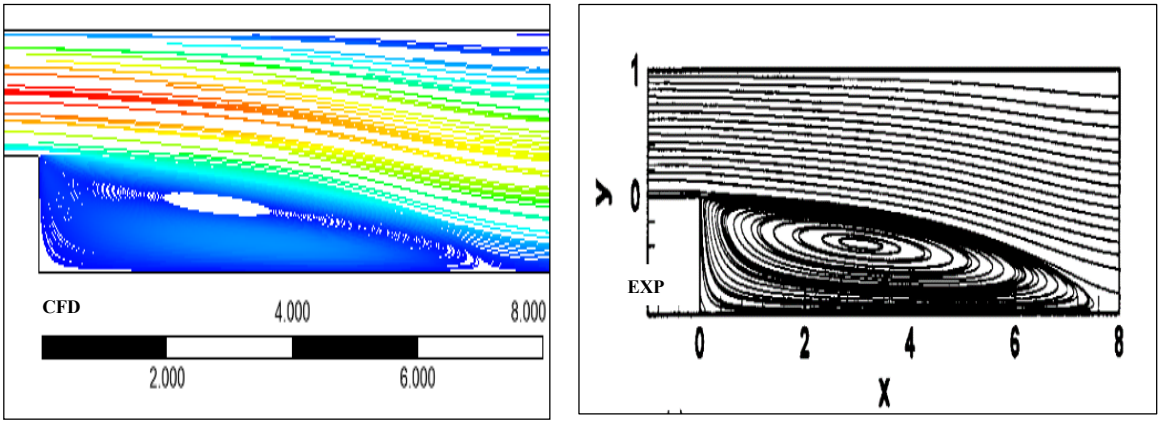

Figure 7. Streamline patterns for the flow separation at Re = 400

4. Result

4.1. Hydrodynamic effect of nanofluid

The distributions of the velocity for different nanoparticle volume fractions for Re=100 and at different sections along the downstream channel are shown in Figures 8-10 for volume fraction ϕ=1, 2, 3, or 4%. The numerical simulations show that the velocity increases as the volume fraction increase at the location x=2, and after the reattachment point the velocity starts to decrease as the volume fraction increases. Two observations are made for the velocity distribution along the downstream wall. The first is for the area between the side wall and the reattachment point, where the result shows that the velocity of the nanoparticles is independent from the sudden expansion and was influenced by the volume fraction, where the velocity increase as the concentration of the particles in the base fluid increases. The second observation after the recirculation zone is that the velocity starts to decrease as the volume fraction increases and that can be seen in Figure 10 at the outlet x=10, and that is shown in Figure 10 at the outlet x=10.

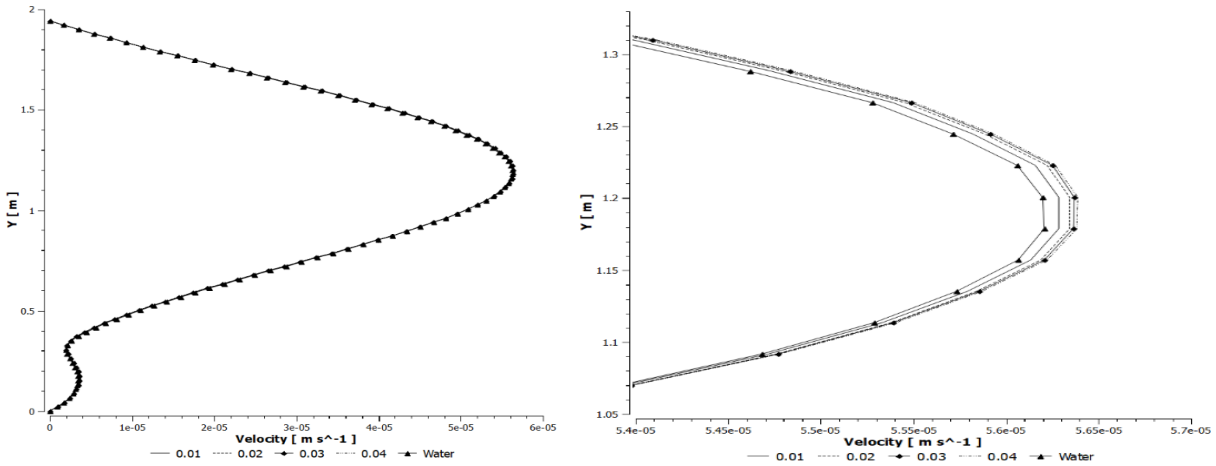

Figure 8. Velocity distribution for different value of volume fraction at x=2m

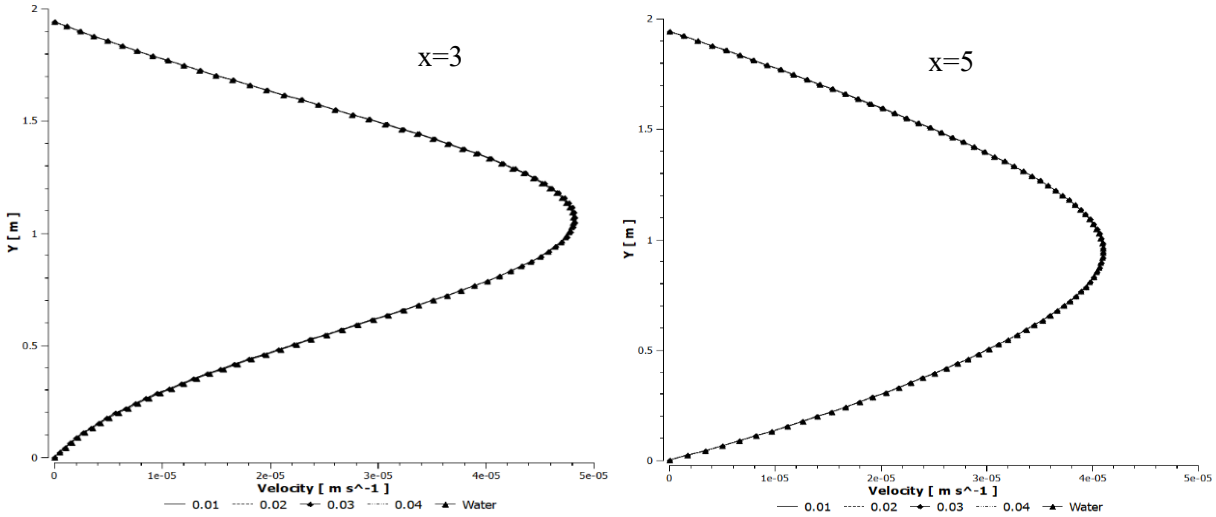

Figure 9. Velocity distribution for different value of volume fraction at x= 3 and at x= 5

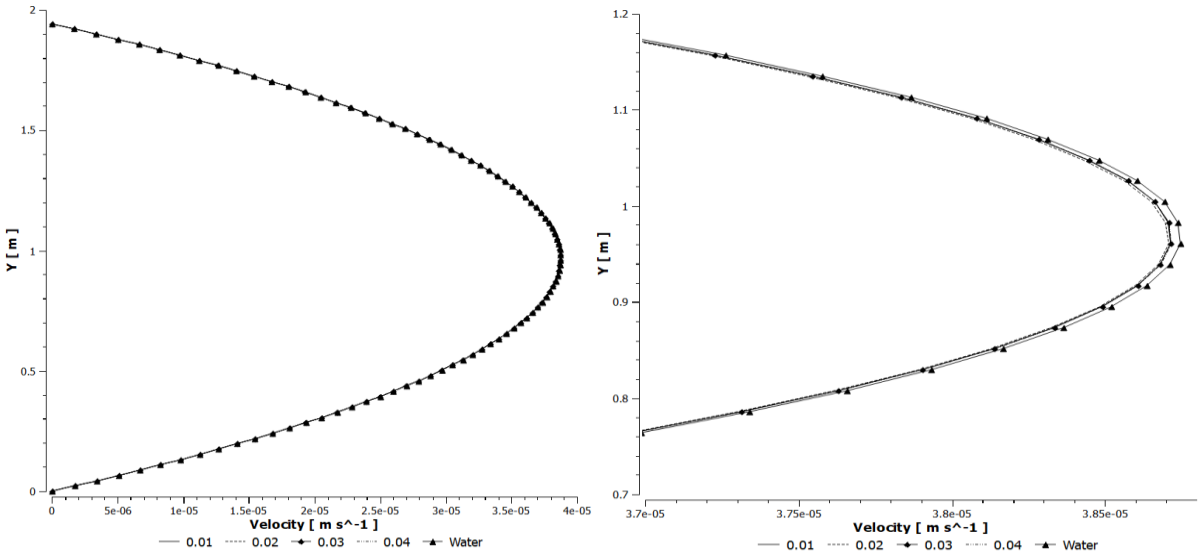

Figure 10. Velocity distribution for different value of volume fraction at x=10

The effect of the volume fraction on the wall shear stress is presented in Figure 9 along the downstream wall. It can be seen that the wall shear stress has negative value in the recirculation zone, where that is due to the reverse flow in that area. The magnitude of the wall shear stress increases as the volume fraction increases. After the reattachment point, the value of the wall shear stress decreases as the volume fraction increases which explains why the velocity in Figure 8 has its maximum value for $\phi = 0.04$. Then, the value of wall shear stress increases with the increase in the concentration of the particles after the velocity profile reattached and redeveloped approaching a fully developed flow. As the fluid flows toward the outlet that effect can be seen in the velocity profile Figure 10, where the water has the highest velocity at the outlet.

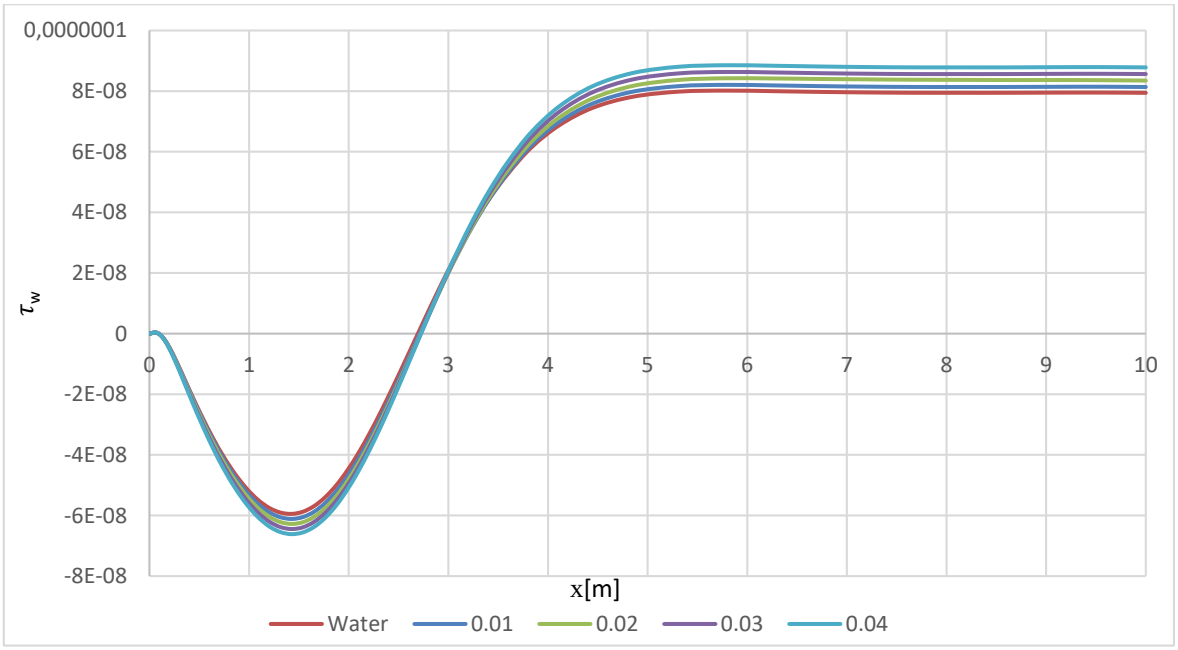

Figure 11. Wall shear stress at different volume fraction along the downstream wall

4.2. Thermal effect of nanofluid

Numerical results for the thermal boundary layers at different locations along the downstream wall are presented. Figures 12-14 present the impact of the nanoparticle volume fraction on the temperature profile for Al_2O_3-water for different concentrations. The thermal boundary layer thickness increases with an increase in the parameter ϕ. Comparison of the temperature profiles for different nanofluid concentration shows that Al_2O_3- water at 0.04 has the thickest thermal boundary layer. Therefore, it is observed that the nanoparticles change the flow and heat transfer characteristics and causes an increase in the thermal boundary layer.

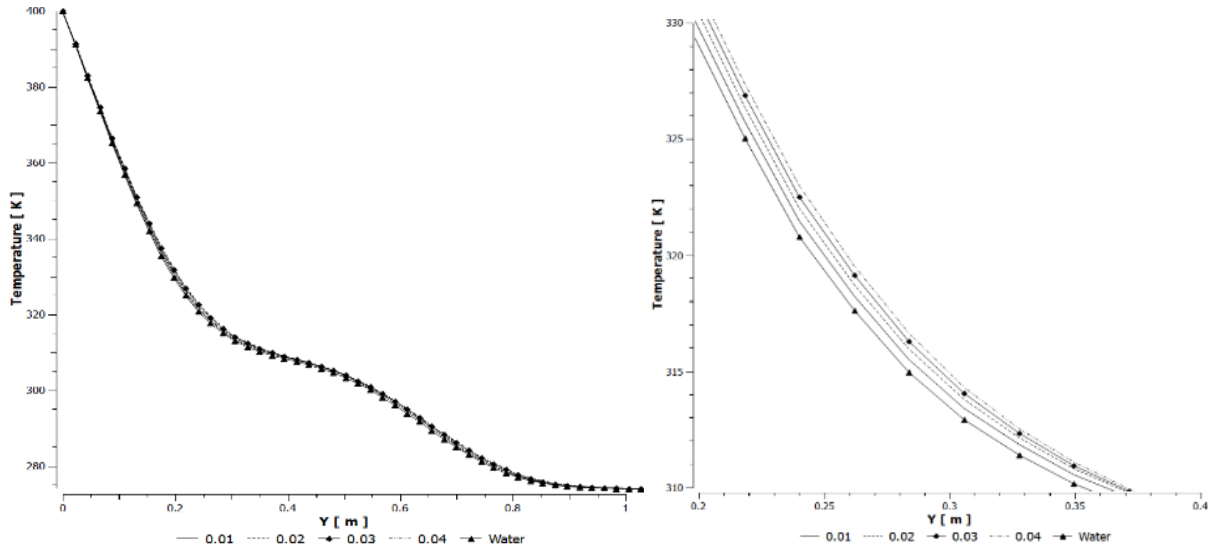

Figure 12. Temperature profile for Al_2O_3 for different value of volume fraction at x=2

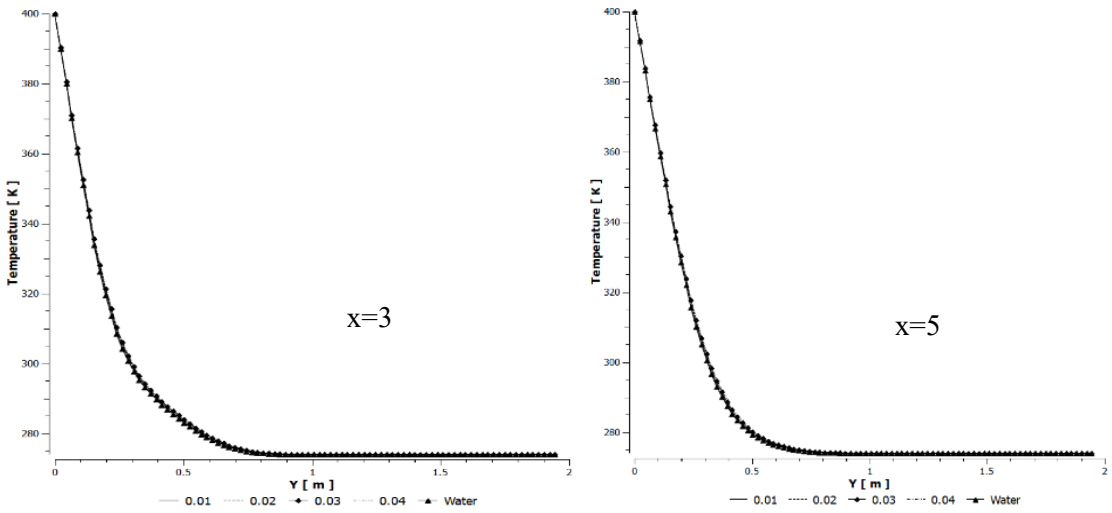

Figure 13. Temperature profile for Al_2O_3 for different value of volume fraction at x=3 and x=5

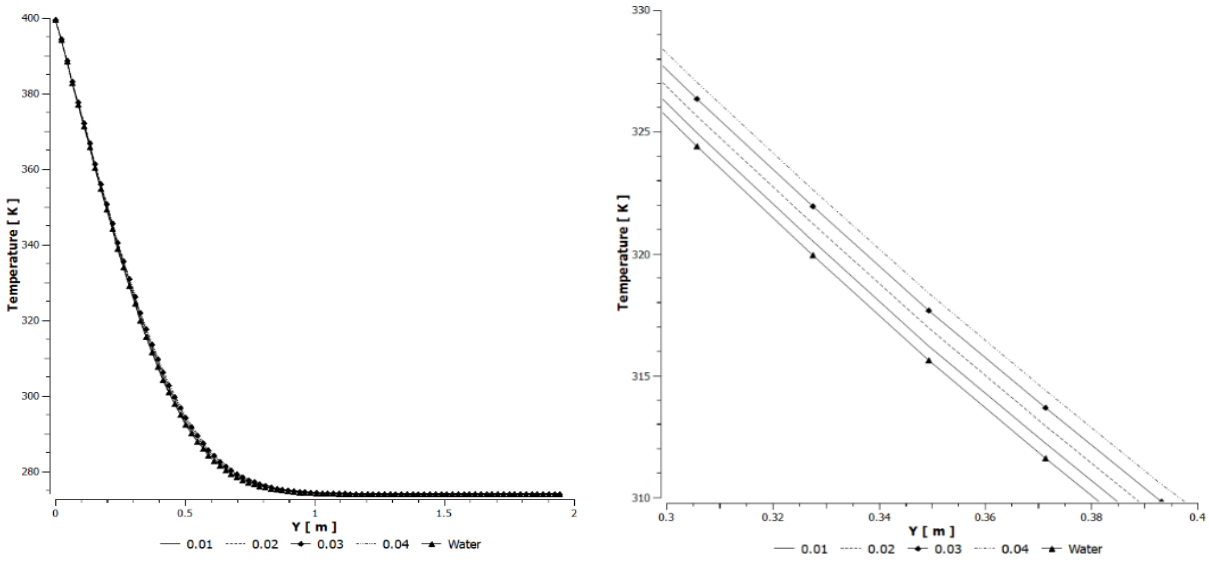

Figure 14. Temperature profile for Al_2O_3 for different value of volume fraction at x=10

The effect of the nanoparticles concentration on the heat transfer is studied and the result is introduced in Figure 15. The result shows the variation of the average heat transfer along the downstream wall for the five-volume fractions tested fluids 0,1,2,3,4 %. It can be observed an improvement in the heat performance with the increase in the volume fraction. The nanofluid with a 4% volume concentration showed the highest heat transfer values along the downstream wall. From the graph, a remarkable increase in the average heat transfer is located in the reattachment point. This increase is due to the increase in the temperature gradient at the lower wall, which implies an increase in the inertia forces, more, the increase in the concentration results in augmentation in the thermal conductivity.

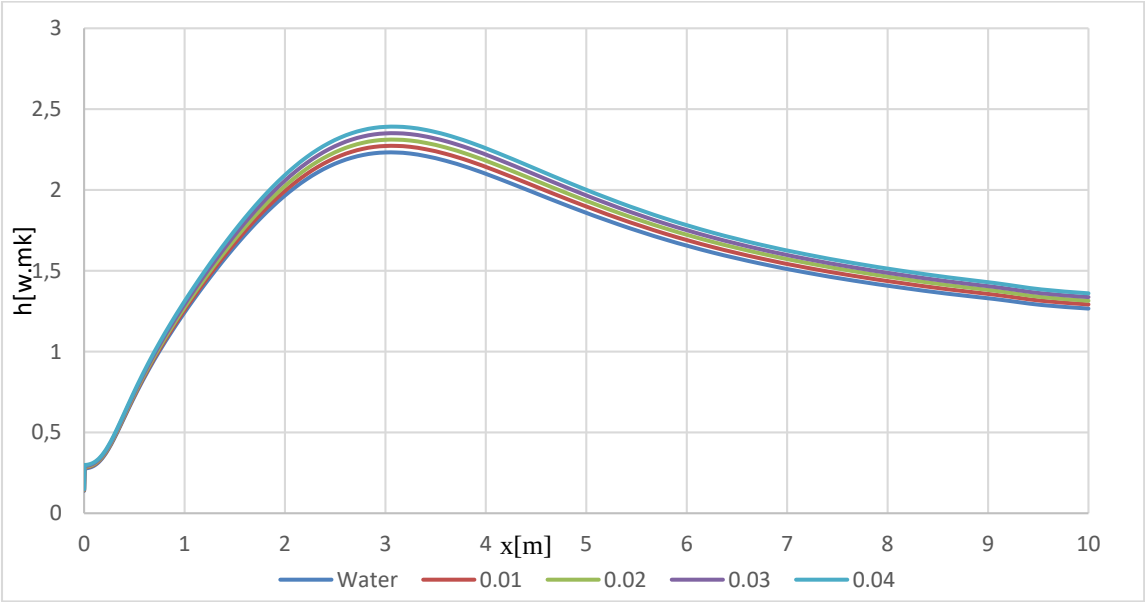

Figure 15. The average heat transfer along the plate (Al_2O_3 -water case)

5. Conclusion

CFD simulations of the forced convection flow over backward facing step were carried out. We can summarize our findings as follows:

The flow reattachment points calculated in this paper have excellent agreement with those obtained experimentally by Armaly et al. [3]. We have an excellent agreement with result got simulation by Biswas et al. [38]. Validating the numerical result with measured data given in [3]. In our paper we have pointed on the impact of the Al_2O_3 nanoparticles in water base fluid. We examined how the velocity distribution, the wall shear stress, the temperature distribution and the heat transfer change with volume fraction of the nanoparticles. The maximum velocity shows an increase with increasing volume fraction at x=2, however at the outlet the impact of ϕ is opposite. It is obtained that the temperature is increased with increasing the volume fraction of Al_2O_3everywhere. The heat transfer is higher when the volume fraction is bigger. For the downstream wall, the highest heat transfer performance was obtained for maximal ϕ of tested fluids. Our aim is to investigate the impact of the nanoparticle's material on the velocity and thermal profiles.

Acknowledgment:

The described study was carried out as part of the EFOP-3.6.1-16-2016-00011 *Younger and Renewing University – Innovative Knowledge City – institutional development of the University of Miskolc aiming at intelligent specialisation* project implemented in the framework of the Széchenyi 2020 program. The realization of this project is supported by the European Union, co-financed by the European Social Fund. The second author was supported by project no. 129257 implemented with the support provided from the National Research, Development and Innovation Fund of Hungary, financed under the K_18 funding scheme.

References

[1] Abu-Mulaweh H I 2003 *Int. J. Therm. Sci* **42** 897
[2] Denhum M K and Patrick M A 1974 *Trans. Instn. Chem. Eng* **52** 361
[3] Armaly B F Durst F Pereira J C F and Schonung B 2006 *J. Fluid Mech* **127** 473
[4] Shih C and Ho C M 1994 *J. Fluids Eng* **116** 228
[5] Chiang T P Sheu T W H and Tsai S F 1997 *Comput. Fluids* **26** 321
[6] De Brederode V and Bradshaw P 1972 *I. C Aero Report* **72** 9
[7] Hertzberg J and Ho C M 1992 *AIAA J* **30** 2420
[8] Tylli N Kaiktsis L and Ineichen B 2002 *Am. Inst. Phys* **14** 3835
[9] Armaly B F Li A and Nie J H 2003 *Int. J. Heat Mass Transfer* **46** 3573
[10] Nie J H and Armaly B F 2004 *Int. J. Heat Mass Transfer* **47** 4713
[11] Hsieh T Y Hong Z C and Pan Y C 2010 *Numer. Heat Transfer* **57** 331
[12] Chiang T P and Sheu T W H 1997 *Numer. Heat Transfer* **31** 167
[13] Aung W 1983 *J. Heat Transfer* **105** 823
[14] Sparrow E M and Chuck W 1987 *Numer. Heat Transfer* **12** 19
[15] Khanafer K Al-Azmi B Al-Shammari A and Pop L 2008 *Int. J. Heat Mass Transfer* **51** 5785
[16] Chen Y T Nie J H Armaly BF and Hsieh H 2006 *Int. J. Heat Mass Transfer* **49** 3670
[17] Kanna P R and Das M K 2006 *Numer. Heat Transfer* **50** 165
[18] Iwai H Nakabe K and Suzuki K 2000 *Int. J. Heat Mass Transfer* **43** 457
[19] Nie J H and Armaly B F 2002 *Int. J. Heat Mass Transfer* **45** 2431
[20] Armaly B F Li A and Nie J H 2002 *J. Thermophys. Heat Transfer* **16** 222
[21] Barbosa J G Saldana and Anand N K 2005 *Int. J. Comput. Meth. Eng. Sci. Mech* **6** 225
[22] Barbosa J G Saldana,. Anand N K and Sarin V 2005 *J. Heat Transfer* **127** 1027
[23] Lan H Armaly B F and Drameier J A 2009 *Int. J. Heat Mass Transfer* **52** 1690
[24] Carrington D B and Pepper D W 2002 *Numer. Heat Transfer* **41** 555
[25] Lin J T Armaly B F and Chen TS 1991 *Int. J. Heat Mass Transfer* **34** 1568
[26] Lin J T Armaly BF and Chen TS 1990 *Int. J. Heat Mass Transfer* **33** 2121

[27] Hong B Armaly B F and Chen T S 1993 *Int. J. Heat Mass Transfer* **36** 3059
[28] Abu-Mulaweh H I Armaly B F and Chen T S 1993 *Int. J. Heat Mass Transfer* **36** 1883
[29] Iwai H Nakabe K Suzuki K and Matsubara K 2000 *Int. J. Heat Mass Transfer* **43** 473
[30] Abu-Nada E 2008 *Int. J. Heat Mass Transfer* **29** 242
[31] Brinkman H C 1952 *J. Chemistry Physics* **20** 571
[32] Mahbubul I M Saidur R and Amalina M A 2012 *Int. J. Heat Mass Transf* **55** 874
[33] Abu-Nada E 2008 *Int. J. Heat Fluid Flow* **29** 242
[34] Khanafer K and Vafai K 2011 *Int. J. Heat Mass Transf* **54** 4410
[35] Xuan Y and Li Q 2000 *Int. J. Heat Fluid Flow* **21** 58
[36] Kakaç S and Pramuanjaroenkij A 2009 *Int. J. Heat Mass Transf* **52** 3187
[37] Oztop H F and Abu-Nada E 2008 *Int. J. Heat Fluid Flow* **29** 1326
[38] Biswas G Breuer M and Durst F 2003 *J Fluid Eng* **126** 362
[39] Abdullah A Alrashed Omid A Akbari Ali H Davood Majid Z Gholamreza A SShabani Ali Reza S and Marjan G 2018 *Physica B: Physics of Condensed Matter* **18** 30141
[40] Mustafa T 2019 *Comput. Meth. Progr. Bio.* **19** 31698